

Effects of torch flame strength on the combustion process in medium-speed gas engines through pre-chamber orifice specifications

ARTICLE INFO

Received: 5 January 2025
Revised: 25 May 2025
Accepted: 27 May 2025
Available online: 10 July 2025

Gas engines are eagerly introduced for the moment to reduce GHG emissions from the marine sector, and could be used by green methane from the methanation process in the future. Pre-chamber-type gas engines burning lean premixture in a main chamber are the mainstream in the medium-speed engine range. Although the ejection behaviour of torch flames from the pre-chamber has a significant impact on the combustion in the main chamber, there are few research examples of confirming the effects of the pre-chamber specifications by actual observation of the combustion process. In this study, a constant-volume chamber was prepared to reproduce the combustion chamber near the top dead centre of a medium-speed gas engine, to visualize its whole combustion chamber, and to investigate the effects of the pre-chamber specifications. The validity of the CFD simulation based on the RANS turbulence model and the possibility of a design index for the ejection strength of torch flames were also examined.

Key words: *gas engine, pre-chamber, torch flame, combustion visualization, CFD simulation, jet intensity*

This is an open access article under the CC BY license (<http://creativecommons.org/licenses/by/4.0/>)

1. Introduction

Acceleration of global warming justifies the Paris Agreement to achieve the carbon neutrality target by 2050. As for the transportation sectors, radical progresses are being made in the development of electrification [29] and e-fuels [5, 16] to decarbonize prime movers in the field of land transportation, but more generous GHG reduction targets were once set for off-road power sources, such as industrial engines and marine engines, because of their long continuous operating time, and high average engine load, which results in the difficulty in electrification. At IMO/MEPC 80 in 2023 [12], however, it was announced that the marine industry would follow the same path as other sectors to accomplish the carbon neutrality by 2050, and mid-term measures were proposed to reduce GHG emissions by 20% to 30% by 2030 and 70% to 80% by 2040, while its target for the introduction of carbon-free marine fuels such as hydrogen and ammonia, which are essential to achieving the carbon neutrality, was set at a mere 5% to 10% of the fuel share by 2030. For the time being, therefore, it is expected that GHG emission reductions will be promoted by introducing low-speed and medium-speed gas engines with natural gas (NG) fuelled [2], and once the production of hydrogen, the raw material for carbon-free fuels, becomes widespread, it is also promising to continue utilising these gas engines using green methane (e-gas) synthesized through methanation [24].

Unlike low-speed marine gas engines, which operate in a two-stroke cycle with premixed or diffusion combustion mode and can be tolerated with modest mean effective pressure [8, 13], a lean-burn premixed combustion gas engine (LBGE, hereafter) has become mainstream [17] in the field of medium-speed range thanks to its less fuel gas compression work, better thermal efficiency by a high degree of constant-volume [15], and lower NO_x emissions.

Nevertheless, medium-speed LBGEs' combustion chamber of c.a. 200 mm or more in bore exceeds the knock limit bore ($\leq \sim \varnothing 100$ mm) of gasoline-fuelled SI engines and forces them to operate within a narrow range of air-to-fuel ratio (AFR) between the knock limit at richer AFR and the misfire limit at leaner AFR [23]. So, avoiding pre-ignition and knocking at higher engine loads, and misfiring at lower loads, has been the major challenge for LBGEs [18, 25, 28]. In addition, regardless of engine loads, excessive cycle-to-cycle variation and unburned fuel emissions are also worrying problems of LBGEs [9, 10].

After all, it is essential to enhance the ignition energy for the premixture in the combustion chamber of medium-speed LBGEs. Two ignition methods are the mainstream for that purpose. One is a spray flame by direct pilot injection of diesel fuel as seen in so-called "dual-fuel" engines [11], and the other is torch flames ejected through the orifices of a pre-combustion chamber (abbreviated as pre-chamber or PC in the study) mounted in the upper centre of the main combustion chamber (MC). The PC-type ignition is preferred for medium-speed LBGEs because it allows the usage of an ignition plug in the PC to realise mono-fuel operation and to be free from NO_x and soot emissions derived from diesel sprays [1]. More specifically, the PC with a dedicated supply path for fuel gas is called an Active PC (APC), and the one without the path is a passive PC. The former has a larger PC volume, realizes the mixture stratification from PC to MC, and strengthens the ignition potential and penetration of the torch flame. The APC is used exclusively for medium-speed LBGEs with a bore of over 200 mm, which requires higher ignition energy. In the APC, many factors such as the ignition energy, the PC volume, and the number and diameter of the orifice openings may affect the ejection behaviour of the torch flame, but these effects have not been clarified quantitatively

enough because of a lack of full observations of in-cylinder phenomena of gas engines.

In the previous study [3], using a constant-volume chamber (CVC) that simulated a combustion chamber geometry near the top dead centre of an APC-type medium-speed LBGE, the authors visualized the ejection process of torch flames in detail and investigated the effects of the orifice specifications on the penetration and spreading angle of the torch flames. It was also shown that the measured results could be reasonably simulated by a 3D-CFD code implemented with a RANS-type turbulence model [22] and a detailed reaction scheme for methane [4]. All the experiments, however, were executed under incombustible MC gas conditions by filling the MC with pure nitrogen since the study focused on the correlation between the PC orifice specifications and the ejection behaviour of the torch flame. So, it is necessary to continue a comparative investigation both experimentally and numerically under combustible MC gas conditions by filling it with CH_4/air premixture to evaluate the effects of the torch flame ejection on the combustion process in the MC.

Considering many experimental and numerical results have accumulated for various types of medium-speed LBGEs [6, 7, 20, 21], it may be worth proposing a practical design index that estimates the ejection strength of the torch flames based on the PC specifications when designing the combustion chamber of an APC-type medium-speed LBGE.

An index for the ejection strength of the torch flame, so-called “jet intensity”, has already been proposed for an APC-type small high-speed gas engine [19], but other than the engine dimensions and speeds, there are non-ignorable differences between APC-type medium-speed LBGEs and the relevant high-speed gas engine. Its fuel injector is located only in the PC instead of the separate fuel supply lines to both chambers, its ignition plug is located near the bottom of the PC instead of near the top of the PC, and so on. So, careful consideration is necessary before applying such an index.

Generally, the correlation between the torch flame ejection intensity and the pre-chamber specifications has not been fully clarified, especially for larger medium- or low-speed LBGEs. The reason can be that almost no studies have been made that have hierarchically classified the factors that can cause the problems of pre-chamber-type gas engines and investigated the true causes step by step. For example, possible causes of excessive cycle-to-cycle fluctuations include variations in the combustion speed due to excessive stretch of the lean premixed flame by the torch flame, excessive turbulence intensity of the pre-chamber flow excited by direct fuel injection and the inflow flux during the compression stroke, and asymmetry of the pre-chamber flow due to the eccentricity of the swirling flow in the main chamber and the above-mentioned complex flux in the pre-chamber. However, since these factors are combined in an actual engine, it is extremely difficult to identify the true cause. Therefore, it is important to first visualize the ejection behaviour of the torch flame in the entire combustion chamber under rather static conditions where there is no inflow flux due to compression or in-cylinder flow in the main chamber, and to understand the influence of the

pre-chamber specifications and the presence or absence of cycle-to-cycle fluctuations.

In this study, from the above perspective, the correlation between the ejection behaviour of the torch flames and the combustion process in the MC was investigated both experimentally and numerically in the same manner as the previous study by filling the MC of the CVC with a CH_4/air premixture. The validity of the jet intensity index was examined by the observed ejection behaviours of the torch flame under comparative conditions with an APC-type medium-speed gas engine based on the PC orifice specifications.

2. Experimental and numerical procedures

2.1. Experimental apparatuses and procedures

Figure 1 and Table 1 show the central cross-section and main specifications of the constant-volume chamber (CVC) used in the study. It is the same as the one used in the authors' previous study [3], so its features are briefly summarised here. The CVC consists of a simple pancake-shaped main combustion chamber (MC) with a bore of $\text{Ø}240$ mm and a height of 30 mm. A pre-combustion chamber (PC) is mounted on the central axis of the CVC's top lid and protrudes to about half the height of the MC. The PC with orifices near its bottom houses an ignition plug and a high-pressure gas injection valve around its top. The configuration well reproduces the clearance volume of a medium-speed LBGE. The PC geometries, such as orifice diameter and the number of orifices, can be changed by replacing a PC tip part attached to the bottom of the PC. The details of the tested PC geometries will be explained later.

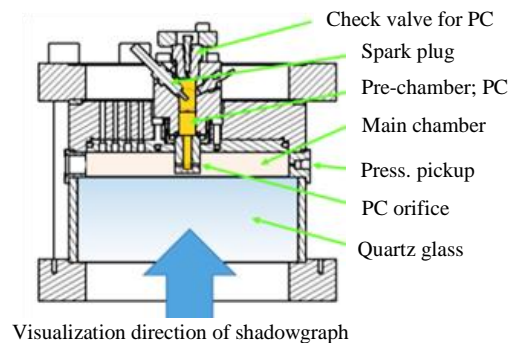


Fig. 1. Cross-sectional views of the CVC

Table 1. Main specifications of CVC

| | |
|---|--|
| Main chamber (MC): $D_{MC} \times H_{MC}$ | $\text{Ø}240 \text{ mm} \times 30 \text{ mm}$ |
| Pre-chamber (PC): $D_{PC} \times H_{PC}$ | $\text{Ø}20 \text{ mm} \times 65 \text{ mm}$ (upper part of PC) |
| Optical window: $D_w \times H_w$ | $\text{Ø}260 \text{ mm} \times 100 \text{ mm}$ Fused quartz glass |
| Max. in-chamber press. | 10 MPa |
| Ignition device in PC | Spark plug |
| Mixture supply system | PC and MC separated |
| Primary for artificial air | $\text{O}_2 + \text{N}_2$ |
| Secondary for fuel gas | CH_4 |

Figure 2 shows a system diagram for blending and supplying the premixture for the MC and the PC of the CVC. Both chambers are independently controlled to simulate an

Active PC type (APC-type) medium-speed LBGE. The system consists of primary mixer tanks blending artificial air from pure O_2 and N_2 , secondary mixer tanks adding methane (CH_4) to the artificial air to prepare a premixture of CH_4 /air, and sets of a solenoid valve and a pressure regulator with a built-in pressure sensor before and after the tanks. The exit of the secondary mixer tank for the PC is connected to the high-pressure gas injection valve to realize the APC-type fuel supply, while the exit of the secondary mixer tank for the MC is connected to the MC directly through a set of solenoid valves and a pressure regulator. An exhaust/vacuum line is also connected to the MC to scavenge the burned gas into a sample bag for emission analysis and to evacuate the whole system for the next experiment. The experimental procedure is as follows. First, two combustion chambers, mixer tanks, and all connection pipes are evacuated. Second, the MC and PC are filled with the component gases up to the specified partial pressure. Third, a thyristor shuts off the current to an ignition coil, and spark ignition happens in the upper part of the PC. At last, after the combustion ends, the burned gas in the CVC is collected into a sample bag for emission analysis. A CPU electronically controls all the solenoid valves and pressure regulators with a specified time sequence. Each pressure regulator is optimized for pressure control accuracy according to the control range.

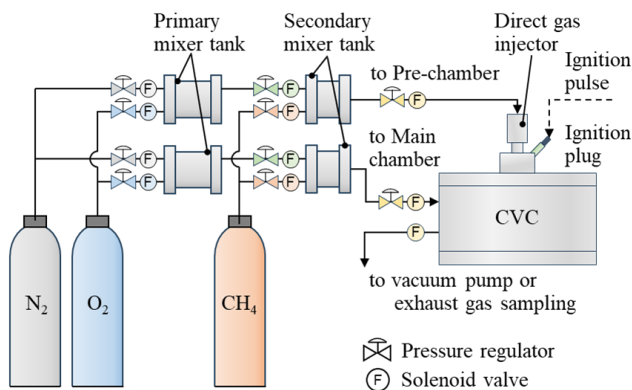


Fig. 2. System diagram for blending and supplying the premixture for the main chamber and the pre-chamber of the CVC

2.2. CFD sub-models and mesh setup

The 3D-CFD simulation by CONVERGE in the previous study by the authors [3] is continuously applied to reproduce the combustion phenomena in the CVC that simulated a chamber geometry of a PC-type medium-speed LBGE. A RANS turbulence scheme based on the RNG $k-\epsilon$ turbulence model is adopted to save computational load and time, considering the larger scale of medium-speed LBGEs and the practical CFD usage in the design phase. As for the combustion-related reactions, the SAGE detailed chemical kinetics solver by Senecal [22] is activated only in cells that pass threshold levels of temperature and HC mole fraction specified in CONVERGE. The multizone chemistry model by Babajimopoulos [4] was used to expedite the detailed chemistry calculations. The reaction mechanism is the reduced version of GRI-Mech1.2 by Kazakov [14] with an enhanced Zeldovich mechanism embedded and consists of

26 species and 107 reactions for methane. The spark ignition in the PC was numerically substituted by the energy source model. The jets of the unburned PC mixture were identified by setting the boundary concentration of marker PC gas to 1.0 mass%, and the torch flames, including the ignited MC mixture, were identified by setting the boundary cell temperature to 350 K or higher.

The meshing strategy was kept the same as the previous study [3], such as the usage of a rectangular Cartesian coordinate instead of a cylindrical coordinate concerning the constraint of axisymmetric alignment due to the central axis setting, but a finer mesh than the previous one was supposed to be necessary for better prediction of the ignition process of the MC premixture by the torch flame and the following flame propagation. The size and the number of the cells were changed as follows. The initial grid interval in the PC volume was halved from 1.0 mm to 0.5 mm. This reduction scheme was the same for a volume of a truncated-cone shape attached to the exit of orifices with a minimum diameter of about 8 mm and with a spread angle of about 30 degrees, while the grid interval in the PC orifices was reduced from 0.5 mm to 0.25 mm. The total number of cells is initially set to c.a. 1.0 million, about 4 times what it was in the previous study. As before, the Adaptive Mesh Refinement (AMR) was activated based on the local gradient in temperature and velocity between the cells, but the minimum grid interval was reduced from 0.5 mm to 0.25 mm and the maximum number of cells was increased from 1.5 million to 20 million, although both parameters were autonomously adjusted by the AMR. All the wall temperatures of the combustion chambers were set to 290 K. The heat loss to the wall surfaces was predicted by the turbulent heat transfer model using the boundary layer treatment based on the nondimensional distance y^+ and the turbulent kinetic energy. For a better understanding of the calculation results, preceding jets of unburned PC mixture and following torch flames should be distinguished from the charge gas or the mixture in the MC. As before, the gas components originating from the PC mixture were identified as marker gases.

3. Experimental conditions

Table 2 lists the experimental conditions for both combustion tests and numerical simulations. Setups for photographing the combustion phenomena in the MC are included in the lower lines of the table.

Table 2. Experimental conditions

| | |
|-----------------------|---|
| PC initial charge gas | CH_4 /air premixture, $\lambda_{PC} = 1.0$ |
| MC initial charge gas | Pure nitrogen ($\lambda_{MC} = 0/0$) Artificial air ($\lambda_{MC} = \infty$) CH_4 /air premixture ($\lambda_{MC} = 1.7$) |
| Charged gas state | 1.0 MPa, 290 K |
| PC geometry | PC1~PC5 on Table 3 |
| Ignition device | Ignition plug in PC |
| Frame rate | 20,000 fps |
| Resolution | 1024×1024 pixels |
| Exposure time | 10.0 μ s |

Table 3. Main specifications of the tested PC geometries

| PC geometry | Orifice specifications | | | | | Throat diameter D_t [mm] | Chamber volume ratio V_{PC}/V_{MC} [%] |
|-------------|------------------------|-------------------|----------------------------|---------------------------|---|----------------------------|--|
| | Diameter D_o [mm] | Length L_o [mm] | Aspect ratio L_o/D_o [-] | Number of holes N_o [-] | Total opening area A_o [cm ²] | | |
| PC1 | Ø3.5 | 7.5 | 2.14 | 8 | 0.770 | Ø15 | 2.3 |
| PC2 | Ø4.0 | 7.5 | 1.86 | 6 | 0.754 | Ø15 | 2.3 |
| PC3 | Ø3.1 | 7.5 | 2.42 | 10 | 0.755 | Ø15 | 2.3 |
| PC4 | Ø2.5 | 7.5 | 3.00 | 8 | 0.393 | Ø15 | 2.3 |
| PC5 | Ø5.0 | 7.5 | 1.50 | 8 | 1.571 | Ø15 | 2.3 |

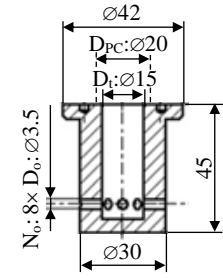


Fig. 3. Cross-sectional view of reference PC geometry (PC1)

Following the typical mixture formation in actual APC-type LBGEs, the PC was always filled with a stoichiometric ($\lambda_{PC} = 1.0$) CH_4 /air mixture to secure stable ignition in the PC and to enhance torch flames, while MC gas conditions changed by the experimental requirements. In the previous study [3], the MC had been filled with pure nitrogen ($\lambda_{MC} = 0/0$) by shutting off a solenoid valve for supplying oxygen to the primary mixer tank and a corresponding valve for CH_4 to the secondary mixer tank. In the case of the combustible MC gas conditions, a CH_4 /air mixture of an equivalence ratio; $\lambda_{MC} = 1.7$ was blended in the secondary mixer tank. Additionally, the artificial air was tried out as an MC charge gas to examine the effects of the continuation of the combustion reactions of the torch flame with a reference PC. Since the detailed investigation had been already done under incombustible MC gas conditions, only the PC geometries for changing the number of orifices and the orifice diameter were selected in this study.

Table 3 summarizes the specifications of tested PC geometries identified as PC1~PC5. PC1 was selected as a reference PC geometry, in which the orifice diameter; D_o is Ø3.5 mm, and the number of orifices; N_o is set to 8.

Figure 3 shows a cross-sectional view of the reference PC (PC1). All the orifices of the PCs are horizontally bored to make it easy to measure the penetration and spread cone angle of the torch flame from the visualized flame images. PC2 and PC3 have N_o of 6 and 10, respectively, and their D_o is determined so that the total orifice opening area is almost the same as that of PC1. For PC4 and PC5, N_o is set constant at 8 and D_o is set to Ø2.5 mm and Ø5.0 mm, respectively.

4. Results and discussion

4.1. Comparison of torch flame developments in various MC in-chamber gas

Although already detailed in [27], it would be better to briefly mention the effects of the MC in-chamber gas's reactivity on the torch flame's development process.

Figure 4 compares the temporal changes in averaged L_f and θ_f of torch flames from the standard PC (PC1) by changing the MC in-chamber gas from nitrogen ($\lambda_{MC} = 0/0$) through air ($\lambda_{MC} = \infty$) to a premixture ($\lambda_{MC} = 1.7$). For reference, observation results of L_f under $\lambda_{MC} = 0/0$ conditions were well approximated to a steady gas jet regardless of the nozzle orifice specifications because it showed the relation of $L_f \propto t^{0.5}$ with time; t on the ASOE basis.

As shown in the figure, L_f was almost the same for $\lambda_{MC} = \infty$ and $\lambda_{MC} = 1.7$ except for the developing stage of

the torch flame, and L_f for $\lambda_{MC} = 0/0$ was shorter than for other in-chamber gases. This suggests that the MC in-chamber gas was entrained into the torch flame immediately after the preceding unburned PC mixture jets out, that the increase in L_f was caused by the flame advance to the preceding unburned PC mixture [26], and that $\lambda_{MC} = \infty$ needed a longer time than $\lambda_{MC} = 1.7$ for the unburned premixture to ignite and merge with the torch flame. In addition, \dot{L}_f at $\lambda_{MC} = 1.7$ was the highest at the start of the torch flame ejection, but it slowed down sharply as the flame developed and became the lowest near 10 ms ASOE.

θ_f was almost constant at around 20 deg. at $\lambda_{MC} = 0/0$ and $\lambda_{MC} = \infty$, whereas θ_f at $\lambda_{MC} = 1.7$ was consistently larger than other λ_{MC} conditions and increased with time, reaching 30 deg. at 10 ms ASOE. This indicates that the flame propagation in the main chamber occurs mainly in the spreading direction, not in the injection direction.

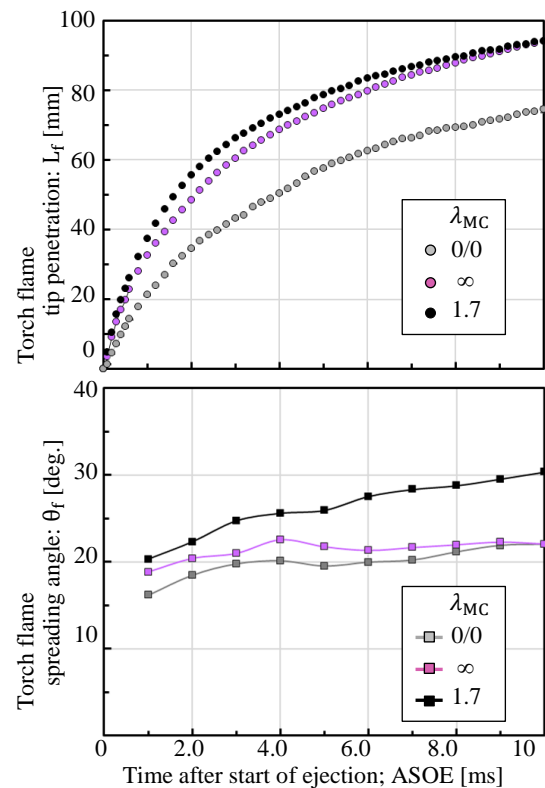


Fig. 4. Effects of the reactivity of the in-chamber gas of the MC on torch flame penetration: L_f (upper half) and its spreading angle: θ_f (lower half) by PC1 with $N_o = 8$ and $D_o = \text{Ø}3.5$ mm

Figure 5 exemplifies the shadowgraph images of the torch flame under the three MC in-chamber gas conditions at 4, 8, and 12 ms ASOE. Reflecting that the MC premixture was entrained in the torch jet and the flame propagation started into the unburned MC premixture, the difference in brightness between the burning region and the background of the shadowgraph was the largest at $\lambda_{MC} = 1.7$ of the three since the torch flame temperature was the highest in the area.

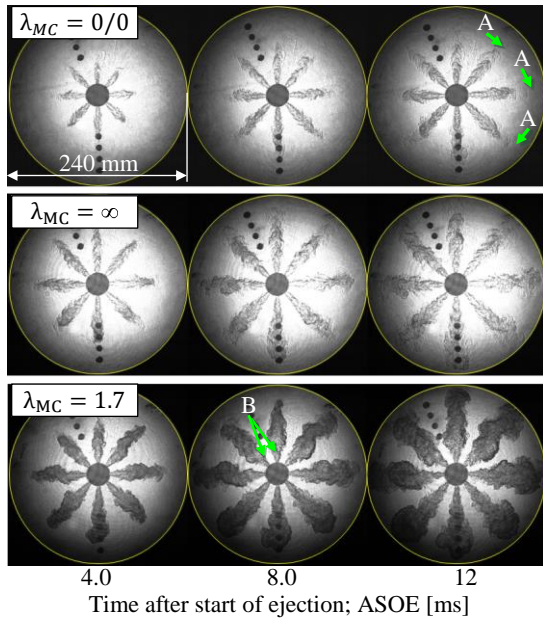


Fig. 5. Ejection behaviours of torch flames under different MC in-chamber gas conditions; $\lambda_{MC} = 0/0$: N_2 (top), $\lambda_{MC} = \infty$: air (middle), and $\lambda_{MC} = 1.7$: premixture of CH_4/air (bottom) with reference PC1 ($N_o = 8$, $D_o = \varnothing 3.5$ mm)

On the other hand, the difference was roughly negligible in $\lambda_{MC} = \infty$ and $\lambda_{MC} = 0/0$. It is inferred L_f at $\lambda_{MC} = 0/0$ was shortened by the ignition difficulty of the preceding pre-mixture jet originating from the PC that was indicated by the arrow “A”’s in the figure. When the flame enhancement mentioned above, after τ_f reached the tip of the PC-originating jet, which included the preceding unburned PC mixture, the entire torch flame transitioned to a spindle-shaped or snake-head profile. It can also be seen that L_f at

$\lambda_{MC} = 1.7$ was equivalent to that at $\lambda_{MC} = \infty$, but flame propagation to the MC premixture mainly progressed in the direction of increasing θ_f . In other words, the earlier combustion in the MC of the CVC, where the mixing and combustion promotion effects of in-chamber flow cannot be expected, is not a pure flame propagation from torch flame as an ignition source, but rather the entrainment and ignition of the premixed air-fuel mixture in the MC by the torch flame proceeds in parallel. Furthermore, as shown by the arrow “B”, it can be noted that L_{fi} of 10~15 mm from the orifice exit was observed in the case of $\lambda_{MC} = 1.7$.

Figure 6 shows the prediction results of the progression of the preceding PC premixture and the following torch flame in the MC during 1~10 ms ASOE under two MC in-chamber gas conditions: $\lambda_{MC} = 0/0$ and $\lambda_{MC} = 1.7$. The unburned premixture from PC is painted in yellow, and the burning region in red. The tip penetration of the PC premixture was roughly the same in both conditions, but L_f at $\lambda_{MC} = 1.7$ was consistently longer than L_f at $\lambda_{MC} = 0/0$ from 1 ms ASOE, that is, immediately after the ejection start of the torch flame. The torch flame at $\lambda_{MC} = 1.7$ then quickly advanced to the tip of the PC-originating mixture, and θ_f also rapidly expanded, as shown in the figure. Although neither τ_{fi} nor L_{fi} was predicted by the simulation, it can be said that many of the considerations based on the observation results were well supported by the CFD, and L_f and θ_f in a combustible MC in-chamber gas were favourably reproduced just as a non-combustible MC in-chamber gas condition.

4.2. Effects of the number of PC orifices

The number of PC orifices: N_o is an important design factor related to the spatial distribution and total surface area of torch flames. PCs of $N_o = 6$ (PC2), $N_o = 8$ (PC1), and $N_o = 10$ (PC3) were selected to investigate the effects of N_o . Each PC geometry has a common V_{PC} and L_o , and its own D_o adjusted to have almost the same A_o . The orifice aspect ratio changes from 1.86 (PC2) through 2.14 (PC1) to 2.42 (PC3). In general, smaller N_o gives larger ejection momentum pre torch flame and longer L_f . The measurement results at $\lambda_{MC} = 0/0$ in the previous study by the authors [3] were consistent with the tendency.

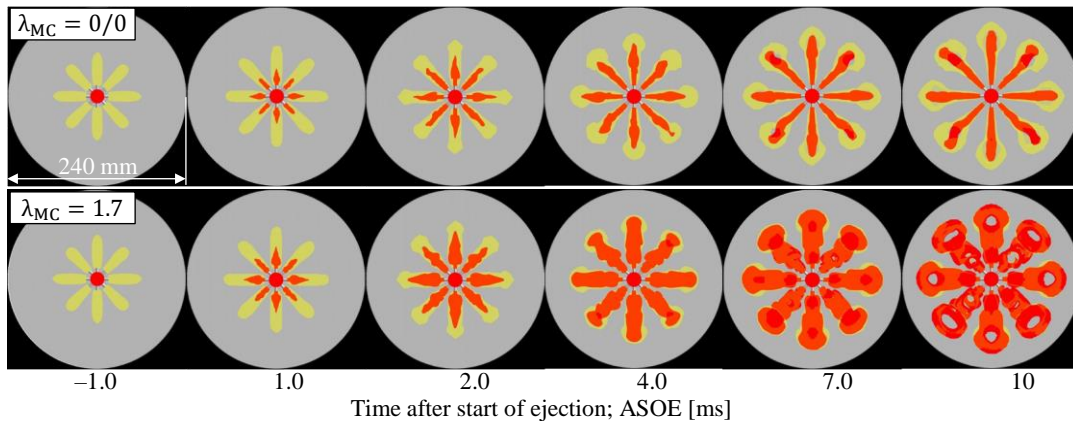


Fig. 6. Effects of MC in-chamber gas on developing process of PC-origin preceding unburned gas jets and torch flame with reference PC1 ($N_o = 8$, $D_o = \varnothing 3.5$ mm) with $\lambda_{MC} = 0/0$ (N_2 , upper row) and $\lambda_{MC} = 1.7$ (pre-mixture of CH_4/air , lower row). Unburned premixture originating from PC painted in yellow and burning region painted in red

Figure 7 shows the temporal changes of L_f and θ_f observed in the tested PCs adding the corresponding changes for PC1 at $\lambda_{MC} = 0/0$ for comparison. The above-mentioned tendency of L_f versus N_o was confirmed again at $\lambda_{MC} = 1.7$. As pointed out in the previous section, \dot{L}_f at the early ejection stage up to 2 ms ASOE was much higher at $\lambda_{MC} = 1.7$ than at $\lambda_{MC} = 0/0$. Still, it can be pointed out

that \dot{L}_f rapidly reduced in the later ejection stage around 10 ms ASOE and the effect of N_{ori} became relatively small when considering L_f at $N_o = 8$ and $N_o = 10$ are almost equal, and L_f at $N_o = 6$ slowed down to near stagnation in the later ejection stage. These can be recognized as the differences from the $\lambda_{MC} = 0/0$ case.

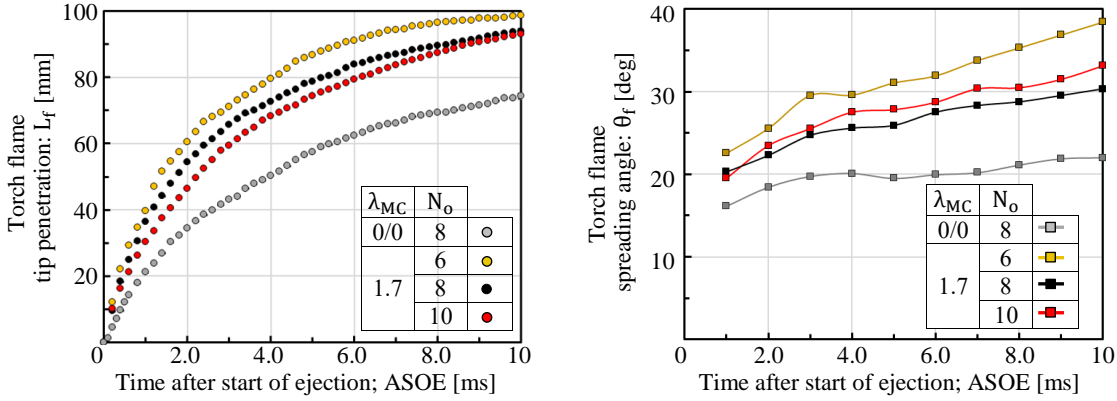


Fig. 7. Effects of number of PC orifices; N_o on torch flame penetration: L_f and its spreading angle: θ_f by PC2 ($N_o = 6$, $D_o = \varnothing 4.0$ mm), PC1 (8, $\varnothing 3.5$ mm), and PC3 (10, $\varnothing 3.1$ mm) respectively with ca. same A_o

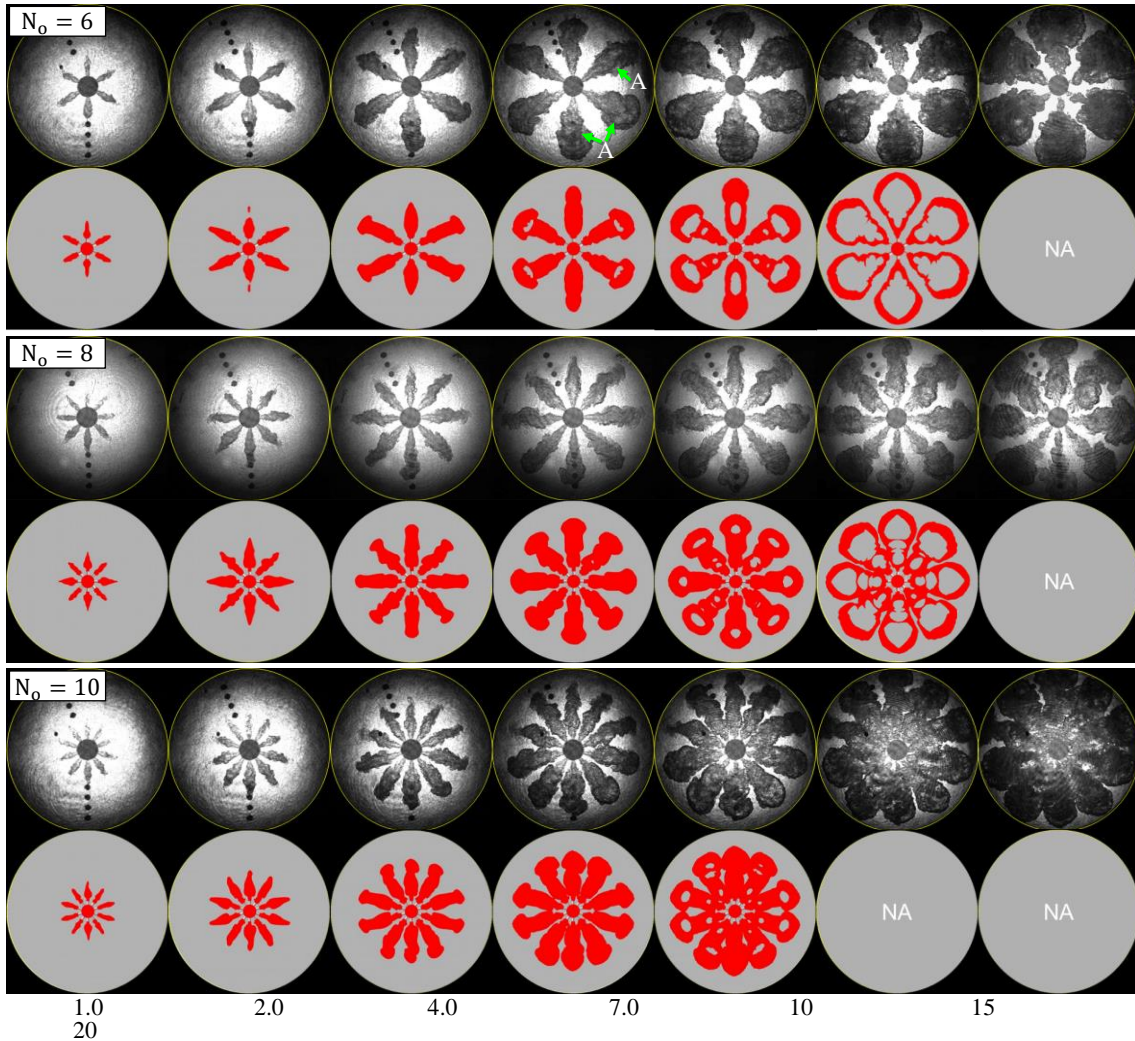


Fig. 8. Effects of the number of PC orifices; N_o on ejection behaviour of torch flame by PC2 ($N_o = 6$, $D_o = \varnothing 4.0$ mm), PC1 (8, $\varnothing 3.5$ mm), and PC3 (10, $\varnothing 3.1$ mm) respectively, with ca. same A_o . Shadowgraph images (upper row of each island) and simulation results (lower row of each island)

On the other hand, the measurement results for θ_f at $\lambda_{MC} = 1.7$ condition were rather different from those at $\lambda_{MC} = 0/0$. At $\lambda_{MC} = 0/0$, the correlation with N_o and the elapsed time in ASOE was weak, and it was found that θ_f was almost constant over time at around 20 degrees regardless of N_o . However, θ_f at $\lambda_{MC} = 1.7$ showed a monotonic increase over time in all N_o cases, and the differences among the tested N_o were more evident. Specifically, the torch flame expanded most rapidly in $\pm\theta_f$ direction in the $N_o = 6$ case, and except for just after the ejection start. θ_f at $N_o = 10$, where the torch flame momentum per PC orifice was the smallest of the three PCs, was slightly wider than θ_f at all N_o cases. In addition, it can be noted that the increase in θ_f at all N_o cases temporarily slowed down after 4 ms ASOE, and then it tended to increase again. This may mean that the torch flame expanded enough to contact the upper and lower walls of the MC as described below.

Figure 8 compares the shadowgraph images of torch flames with the predicted ones for the three N_o settings. To consider the correlation with the heat release process, the display period is set to 1~20 ms ASOE. In most of the prediction results after 15 ms ASOE, however, the flame image was not available because of the discontinuity of the isothermal surface of 350 K. The considerations of the shadowgraph images can be summarized as follows.

As a general trend, τ_{fi} was about 1~2 ms regardless of N_o , but τ_{fi} of each torch flame captured in a certain shadowgraph image at 1 ms ASOE indicated τ_{fi} varied among the torch flames. The unburned MC premixture between the torch flames seemed hard to burn up at any N_o even in the later combustion stage in the MC. As in the images at least after 10ms ASOE, when the tip of the torch flame came into contact with the upper and lower MC walls and flattened out, the apparent θ_f became overestimated.

The influence is stronger at $N_o = 6$, where the volume of the torch flame alone was the largest of the three cases, and there were flame images in which the original torch flame could be distinguished inside the flattened flame near the wall (arrow "A"s). By excluding this apparent expansion of θ_f , a smaller number of orifices such as $N_o = 6$ can increase both L_f and θ_f , but the total contact area between the MC premixture and the torch flames does not grow because of the limitation of the flame growth in $\pm\theta_f$ direction, while with a bigger number of orifices such as $N_o = 10$, the surface area of the torch flame can increase, but a decrease in the penetrating momentum of each flame presumably offsets this merit. Furthermore, at $N_o = 10$, the torch flames from the orifices in the upper half of the shadowgraph image had shorter τ_{fi} by about 1 ms than the orifices in the lower half, and in the downstream of L_{fi} , the torch flames made the immediate and discontinuous transition to the expanding flame profile. This is thought to be the reason why θ_f at $N_o = 10$ was evaluated to be larger than that at $N_o = 8$. Torch flames with shorter τ_{fi} at $N_o = 10$ also lost their penetrating momentum more quickly, and they did not seem to reach the inner sidewall of the MC and resulted in very slow flame propagation to the end gas zone of the MC.

In the CFD prediction, it should be pointed out that L_f is slightly underestimated, τ_{fi} and L_{fi} cannot be reproduced,

so the torch flame expanded immediately after ejection from the PC, and the asymmetric flame development due to the rectangular mesh is particularly noticeable in the case of $N_o = 6$. However, the above-described effects of N_o on the ejection behaviour of the torch flame and the subsequent combustion process are qualitatively reproduced including the flame interconnection in the downstream of L_{fi} at $N_o = 10$. In addition, by the 10 ms ASOE, the holes in the background colour appeared around the flame tip in all N_o cases. This is because the torch flames being in contact with the upper and lower walls of the MC were cooled down and the isothermal surface of the burning area became discontinuous. It supports the wall contact and flattening of the torch flame described above.

Figure 9 shows the temporal change of the rate of heat release (ROHR) for the three N_o settings. The black curves are the estimated ROHRs based on the measured in-chamber pressure, and the red curves are the calculated ones based on the numerically predicted in-chamber pressure.

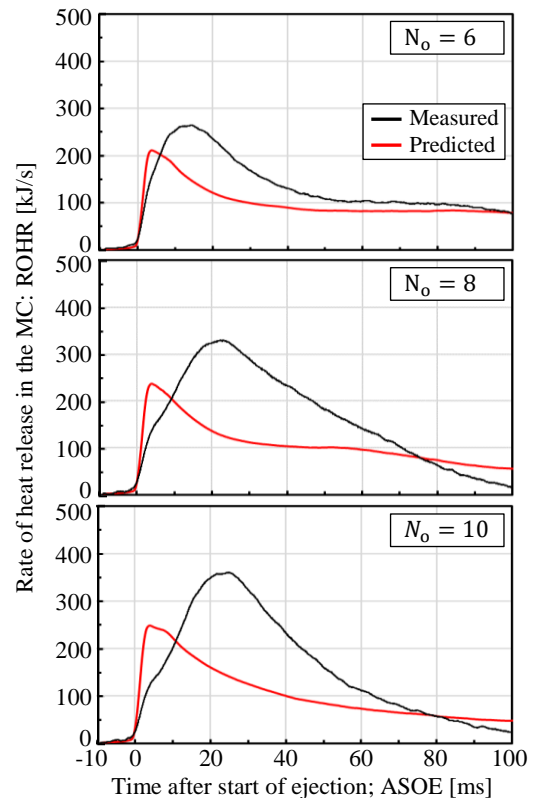


Fig. 9. Effects of the number of PC orifices; N_o on ROHR in the MC by PC2 ($N_o = 6$, $D_o = \varnothing 4.0$ mm), PC1 (8, $\varnothing 3.5$ mm), and PC3 (10, $\varnothing 3.1$ mm) respectively, with ca. same A_o . Measured ROHRs (black curves), and simulated ROHRs (red curves)

First, considering the measured ROHR under the condition of near constant A_o , it can be said that the effects of N_o on the heat release process in the MC was relatively small, and similar ROHR curves derived in all cases. When N_o increased from 6 to 10, the maximum value of the heat release rate increased from 270 kJ/s to around 360 kJ/s, and τ_{HRmax} was delayed from 15 ms ASOE to around 25 ms ASOE. Additionally, there was an inflection point in each

ROHR curve around 5 ms ASOE regardless of N_o , which means the combustion in the MC may temporarily stagnate in the process of flame development. The smaller the number of orifices was, the higher the ROHR around 5 ms ASOE and the steeper the gradient of the ROHR were.

All in all, with a small number of nozzle holes, the increased penetrating momentum per torch flame can promote the early stage of the combustion in the MC, but the effect is not enough to compensate for the decrease in flame surface area and the enlargement of the gap between the torch flames from middle to late stage of the combustion in the MC. With a large number of nozzle holes, on the other hand, early-stage heat release in the MC slows down because of the slow ejection speed of torch flames, but the following heat release can be partially ensured thanks to an increase of the flame surface and a decrease of the gap between the torch flames. However, the penetrating momentum per torch flame seems crucial especially for the late stage of the combustion because the unburned premixture in the end gas zone needs a forcing ignition source to burn up fast instead of the slower flame propagation of the leaner CH_4 -air mixture.

Next, comparing the predicted ROHRs with the measured ones, the tendency was consistent for the maximum ROHR to be proportional to N_o , but the large discrepancy should be noted because the maximum value itself was significantly lower than the measured one and t_{max} advanced to about 4 ms ASOE. As for the total heat release, some trial calculations were executed up to several hundred milliseconds on ASOE, and the total amount of the predicted heat release was ensured to be almost equal to the accumulation of the measured values. The discrepancy may be due to the lack of implementation of appropriate sub-models to reflect the effects of turbulent mixing of the torch flame and the MC premixture that can cause the quench of flame kernels and the resulting extension of τ_{fl} . Moreover, there was a lack of reproducibility of the instantaneous cooling loss around the torch flame including the inner wall of the orifice.

4.3. Effects of diameter of PC orifices

From the results of the previous section, it seems to be important for a large-scaled engine such as APC-type LBGEs, to secure the proper range of N_o so that the gap between adjacent torch flames is neither too broad to propagate nor too narrow to entrain the premixture, and the penetrating momentum of the torch flame to reach the torch flame to the end gas zone of the MC for rapid combustion completion.

In the section, three PCs having $N_o (= 8)$ and V_{PC} in common, but different D_o were tested. Combinations of the PC geometry and D_o were PC4 ($D_o = \varnothing 2.5$ mm), PC1 ($\varnothing 3.5$ mm), and PC5 ($\varnothing 5.0$ mm), respectively. The A_o ratio of PC4: PC1: PC5 was approximately 1:2:4 and the L_o/D_o ratio, which was found to have a positive correlation with the torch flame directionality at $\lambda_{\text{MC}} = 0/0$, was set to 3.0, 2.14, and 1.5, respectively. The display range of the figures is the same as in the previous section unless otherwise specified.

Figure 10 shows the temporal changes in L_f and θ_f for the tested PCs including those for PC1 at $\lambda_{\text{MC}} = 0/0$. The

previous measurements with the same PCs at $\lambda_{\text{MC}} = 0/0$ showed that the smaller D_o was, the longer L_f and the narrower θ_f were. The similar trend existed at $\lambda_{\text{MC}} = 1.7$ in the early stage of torch flame ejection. However, L_f was approximately 1.6 times as long as that of $\lambda_{\text{MC}} = 0/0$ at 2 ms ASOE and about 1.3 times at 10 ms ASOE.

The L_f elongation was particularly noticeable in $D_o = \varnothing 2.5$ mm case, in which the torch flames collided with the inner circumferential wall of the MC around 6 ms ASOE, while the other D_o cases took much more time to reach the wall since the decrease in \dot{L}_f became clear around that timing. Specifically, \dot{L}_f in $D_o = \varnothing 5.0$ mm case decreased rapidly after 3 ms ASOE, and L_f at 10 ms ASOE was the shortest compared to other PC geometries.

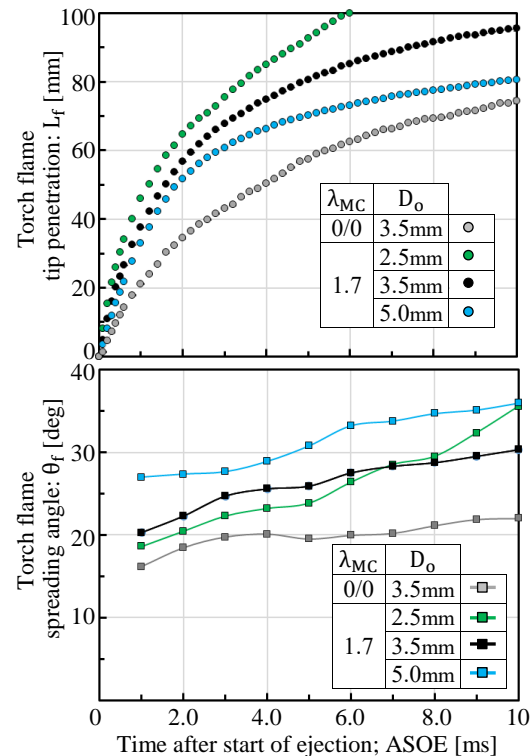


Fig. 10. Effects of diameter of PC orifices; D_o on torch flame penetration: L_f and spreading angle: θ_f by PC4 ($D_o = \varnothing 2.5$ mm), PC1 ($\varnothing 3.5$ mm), and PC5 ($\varnothing 5.0$ mm)

As for θ_f , the flame growth in $D_o = \varnothing 2.5$ mm case was remarkable, too. Although the case showed the smallest θ_f at the beginning of ejection, its θ_f increased rapidly enough to surpass θ_f in $D_o = \varnothing 3.5$ mm case after 7 ms ASOE, when the torch flame in $D_o = \varnothing 2.5$ mm case had already reached the MC inner wall, and to surpass θ_f in $D_o = \varnothing 5.0$ mm case after 10 ms ASOE. In $D_o = \varnothing 5.0$ mm case, the initially large θ_f showed a rapid increase during 4~6 ms ASOE, and it tended to transition to a gradual increase. All of these suggest that the combustion phase ignited by torch flames is greatly influenced by the ejection speed or strength of the torch flame.

Figure 11 compares the shadowgraph images of the torch flame with the predicted flame images for the three orifice number settings. Due to insufficient optical system adjustment in the case of $D_o = \varnothing 2.5$ mm and $D_o = \varnothing 5.0$ mm,

false information was superimposed in the shadowgraph images as a darkened area of about twice the PC radius around the PC (arrow “A”s). It is clear from the shadowgraph images that the smaller D_o or the higher the torch flame ejection velocity, the longer L_{fi} is. In particular, $D_o = \varnothing 2.5$ mm case seems to be worth mentioning in detail.

In the $D_o = \varnothing 2.5$ mm case, ignition of the MC premixture entrained in the torch flame was first observed as late as after 3 ms ASOE, and τ_{fi} and L_{fi} were the longest among the three D_o parameters, but the variation in τ_{fi} and L_{fi} of each torch flame was also considerably large. For example, the τ_{fi} reached as long as 10 ms ASOE for the torch flame that ejected out vertically downwards in the images for $D_o = \varnothing 2.5$ mm case (arrow “B”). On the other hand, the initial value of L_{fi} from the orifices located in the upper half of the same images tended to be about half of L_f (arrow “C”s) rather than the vicinity of L_f like any PCs with other D_o or N_o (arrow “D”s). After τ_{fi} , the flame propagated rapidly from L_{fi} to the lower section of the torch flame, and the section including the entrained MC premixture expanded at the same time. After the ignition, the torch flame

reached the inner circumferential wall of the MC by 10 ms ASOE, but even considering the change in the penetrating direction along the inner MC wall due to the collision, the growth of the torch flame to $\pm\theta_f$ direction accelerated in the middle combustion stage in the MC (arrow “E”). In summary, with an enhanced ejection speed of $D_o = \varnothing 2.5$ mm case, the MC premixture both in the gaps between the torch flames and in the end gas zone was able to be burned efficiently. The latter premixture is important to keep combustion efficiency high because of its large volume contribution in an MC. Upon closer observation, it is clear that L_f fluctuated over time even for torch flames from the same orifice. For example, the torch flame ejecting in the 45° direction to the lower right in the images showed $L_{fi} \approx 55$ mm at 4 ms ASOE but $L_{fi} \approx 68$ mm at 10 ms ASOE (arrow “F”s) when the pure torch flame seemed to push down the post-ignition premixed flame part to the lower side. The torch flame ejected vertically downward in the image had the longest L_f and τ_{fi} and the torch flames advancing to the lower left and right 45° bent upward after 7ms ASOE (arrow “G”s).

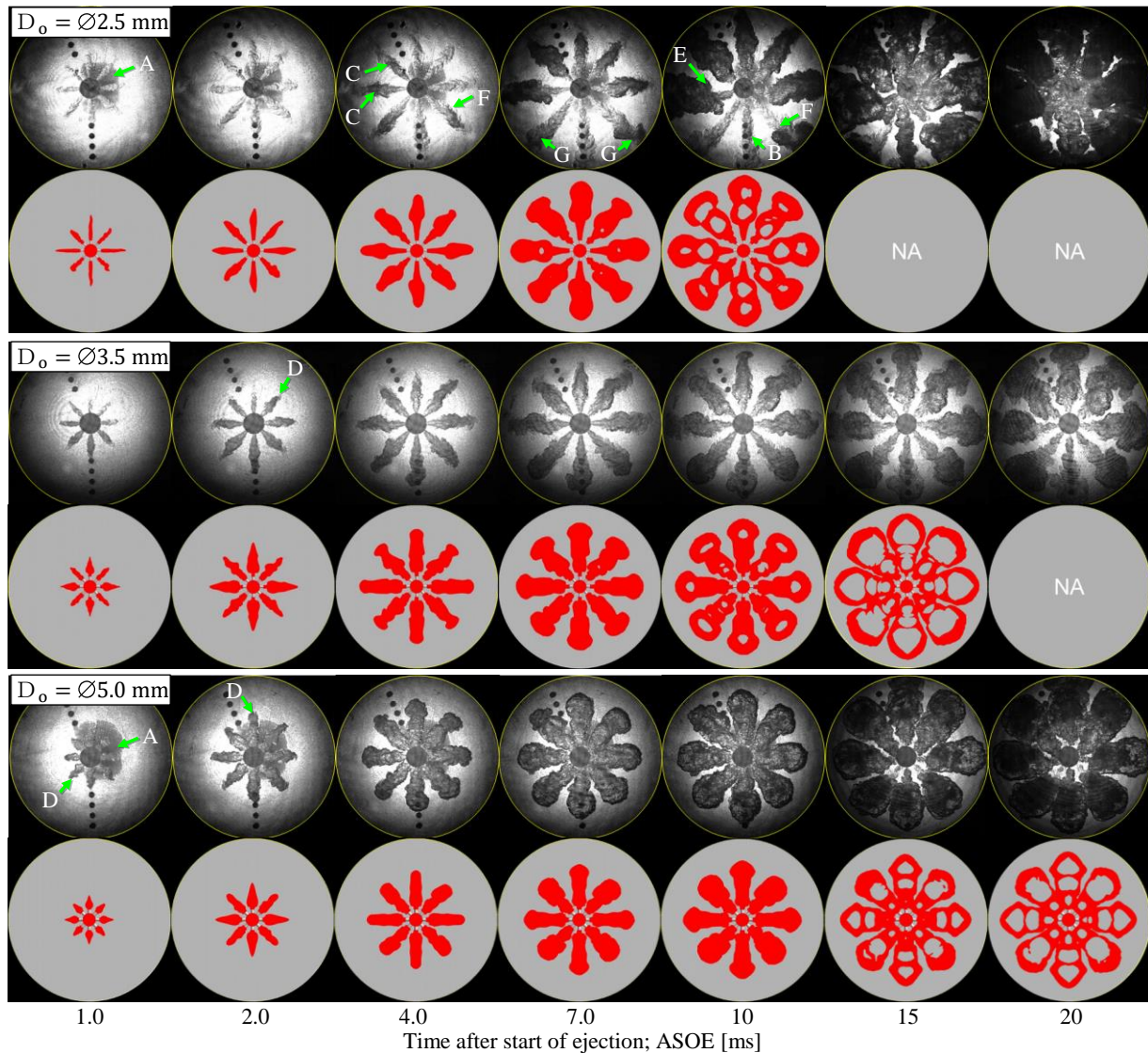


Fig. 11. Effects of diameter of orifices; D_o on ejection behaviour of torch flame by PC4 ($D_o = \varnothing 2.5$ mm), PC1 ($\varnothing 3.5$ mm), and PC5 ($\varnothing 5.0$ mm). Shadowgraph images (upper row of each island) and simulation results (lower row of each island)

One possible explanation goes below. In this experiment, the torch flames in the image's upper half ignited and grew more quickly than the ones in the lower half. A strong secondary in-chamber flow was induced from the upper to the lower half, passing through the MC centre. This downward flow reduced the relative speed between the torch flame and the MC premixture and resulted in the extension of the L_f and τ_{fi} of this torch flame. After the in-chamber flow collided with the peripheral MC wall, the flow split to the right and left and bent two torch flames.

On the other hand, at $D_o = \varnothing 5.0$ mm, τ_{fi} and L_{fi} were extremely short compared to the other PC orifice specifications, and the flame expanded immediately after L_{fi} , and quickly transitioned to a turbulent jet flame with a snake-shaped tip. Overall, the flame development process was similar to that of $N_o = 10$, where the momentum per torch flame was small. However, compared with $N_o = 10$ case, the variation in τ_{fi} , L_{fi} , and development behaviour of the torch flame between each orifice were extremely small, and the decrease in \dot{L}_f in the later stages of combustion was more evident due to the lowest ejection speed. Since the torch flame did not reach the peripheral inner MC wall or the premixture in the end gas zone, even at 20 ms ASOE, it can be inferred that combustion in the later stages was extremely slow.

Regarding the numerical prediction, it must first be pointed out that there was a large discrepancy between the observation results and the numerical prediction at $D_o = \varnothing 2.5$ mm. For the reasons mentioned above about the CFD setup in this study, τ_{fi} and L_{fi} were configured to be zero regardless of the orifice specifications. This means the influence was greater in $D_o = \varnothing 2.5$ mm case, where the absolute values of τ_{fi} and L_{fi} were long and varied depending on the nozzle hole and the elapsed time ASOE. There was also a clear tendency for L_f to be underestimated. On the other hand, at $D_o = \varnothing 5.0$ mm, where τ_{fi} and L_{fi} were the shortest of all the cases, the behaviour of the torch flame ejection and its development was relatively well reproduced by the current CFD setups.

Figure 12 shows the temporal change in ROHR for the three D_o settings. The line type and legends are the same as in Fig. 9, but the scale for the ROHR is doubled. Considering the measured ROHRs, the impact of D_o on the combustion in the MC was considerably high with constant N_o . In $D_o = \varnothing 2.5$ mm case with long τ_{fi} and L_{fi} , the ramp-up of ROHR was modest after the ejection started, but ROHR increased rapidly after τ_{fi} and t_{max} was reached at about 20 ms ASOE with the maximum value just over 1000 kJ/s, which was very high compared to other tested PC geometries.

However, there was also a local maximum value near 13 ms ASOE reflecting that the torch flames were divided into two groups, ones with relatively short τ_{fi} and the others with long τ_{fi} . In addition, the ROHR went negative after 50 ms ASOE, which suggested that the torch flame reached the peripheral inner MC wall at 10 ms ASOE causing the combustion of the entire MC including the end gas zone to be completed fast and that the heat loss through the wall surface increased due to the contact of torch flames with the inner wall.

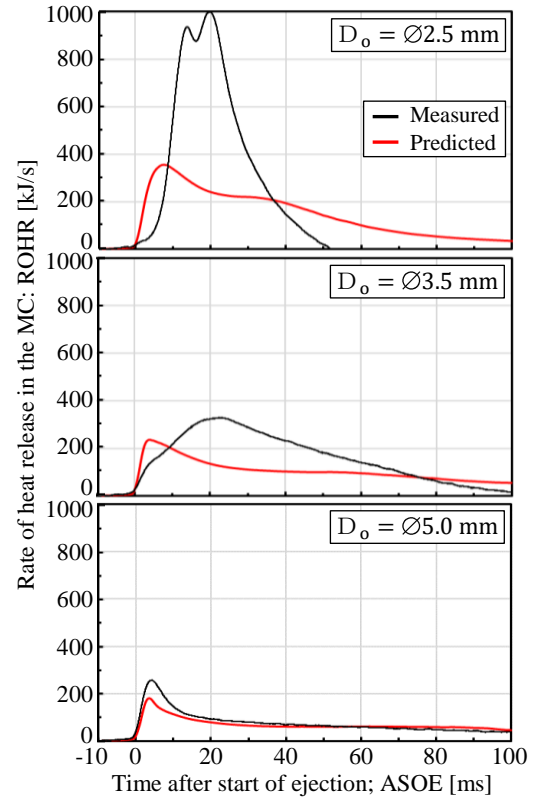


Fig. 12. Effects of diameter of PC orifices; D_o on ROHR in the MC by PC4 ($D_o = \varnothing 2.5$ mm), PC1 ($\varnothing 3.5$ mm), and PC5 ($\varnothing 5.0$ mm). Measured ROHRs (black curves), and simulated ROHRs (red curves)

On the other hand, in $D_o = \varnothing 5.0$ mm case, the ROHR rose fastest because of its short τ_{fi} , and t_{max} was reached at around 4.5 ms ASOE, which was significantly earlier than the PCs of other specifications, but the maximum ROHR was the lowest at just under 260 kJ/s. By comparing with the visualization results shown in Fig. 11, the quick rise of ROHR corresponded to the shortest τ_{fi} and the quick profile transitions to a snake-head shape, and the poor heat release in later stage combustion corresponded to the difficulty for the torch flame in reaching the inner MC wall due to insufficient penetrating momentum.

Next, considering the predicted ROHR, the smaller the D_o was, the lower the ROHR at the beginning of ejection and the higher the maximum ROHR were, both of which were consistent with the visualization results. However, the maximum ROHR was underestimated and t_{max} was overestimated, as in the results in the previous section. A discrepancy in both factors became large, especially in the case of $D_o = \varnothing 2.5$ mm so it was hard to say the reproducibility of the combustion in the MC is appropriate. On the other hand, in $D_o = \varnothing 5.0$ mm case, the discrepancy between the measured value and the predicted one was the smallest in the tested group of PCs, and the predicted ROHR followed a similar trajectory to the measured one, although the maximum ROHR was slightly underestimated. This suggests that the CFD setup applied in the study was capable of relatively good reproduction of the combustion process when the ejection velocity of torch flame was low and the effects of turbulent mixing were small, and that in APC-type methane-air premixed combustion including in actual

engines, flame quenching or τ_{fi} extension due to turbulent mixing between the ejected torch flame and the MC pre-mixture, and the following combustion promotion were essentially important matters.

4.4. Examination of the index for torch flame intensity

Nada et al. proposed the jet intensity: I_b expressed by the following formula [21] for the high-speed small gas engine. The variables in the formula conform to the notation adopted in this paper. The meanings of each factor are listed as follows: V_{PC} : Stored energy in PC (λ_{PC} is usually fixed around unity), $N_o \pi D_o^2/4$: Total opening area of PC orifices, D_{MC} : Distance to the end gas zone (relative evaluation factor).

$$I_b = \frac{V_{PC}}{D_{MC} N_o \pi D_o^2/4} [-] \quad (1)$$

The following can be inferred about the PC specifications of APC-type gas engines. As mentioned in the previous study [3], there are mechanical constraints on V_{PC} and D_t that are almost subordinate to D_{MC} [3]. N_o mainly determining the gap between the torch flames has little freedom to change between reducing the distance for flame propagation to the adjacent torch flame and yet securing space for the torch flame to entrain the MC lean premixture. Considering that V_{PC} is approximately proportional to the cube of D_{MC} and D_o is roughly proportional to D_{MC} , I_b can be regarded as an evaluation index not based on the engine scale.

Under these conditions, it is important to select proper D_o , so that the torch flame can have sufficient initial speed to reach the vicinity of the end gas zone during τ_{fi} , with which I_b is also thought to have positive correlation, and to promote combustion in the entire MC. In this study, for compensation of the change of the orifice aspect ratio that is accompanied with changes in N_o and D_o , the following torch flame intensity is used to confirm the correlation with the measurement results in the CVC.

$$TI = \frac{4V_{PC}(L_o/D_o)^{0.5}}{D_{MC}N_o\pi D_o^2} [-] \quad (2)$$

The term $(L_o/D_o)^{0.5}$ represents torch flame directionality. The evaluation of the effect is based on the measurement results of the ejection behaviour of torch flame under $\lambda_{MC} = 0/0$ conditions.

Figure 13a–f summarizes the investigation of the correlation between the above TI and the various combustion-relating characteristics in the MC obtained in the study.

First, the correlation between TI and the L_f at the ejection end was investigated. The end of ejection was identified as the timing when the differential pressure between them goes to zero. The timing was around 6 ms ASOE for most of the PCs except for 7 ms ASOE for PC4 ($D_o = \varnothing 2.5$ mm) and 4 ms ASOE for PC5 ($\varnothing 5.0$ mm), of which L_f increased less than 7 mm even at 6 ms ASOE. As shown in (a), a linear correlation was found between TI and the L_f at the ejection end. This sustains the validity of the index to indicate the ejection strength of the torch flame.

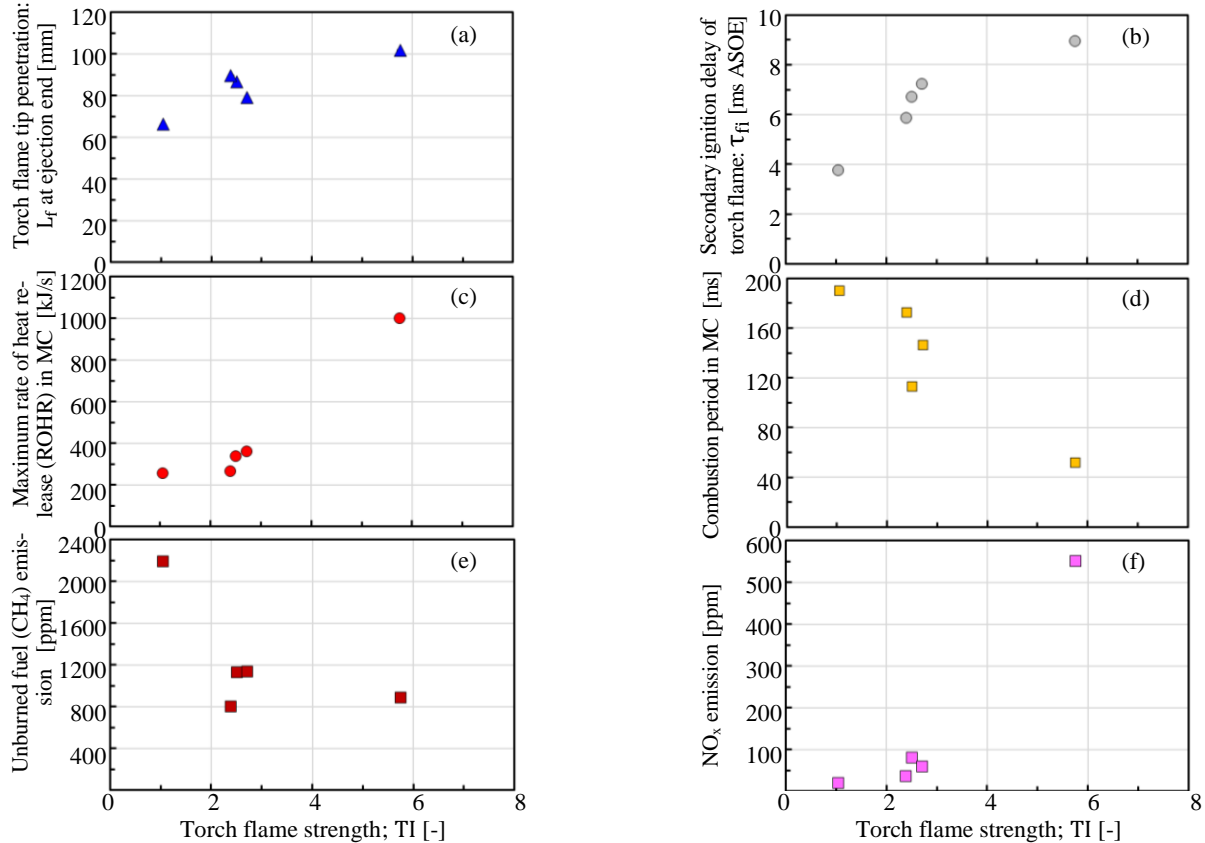


Fig. 13. Correlations between an index for torch flame strength; TI and several combustion and emission characteristics in the MC of the CVC. (a) penetration length of torch flame: L_f at ejection end, (b) secondary ignition delay of torch flame in the MC: τ_{fi} , (c) maximum rate of heat release: ROHR, (d) combustion period in the MC, (e) unburned fuel (CH_4) emissions, and (f) NO_x emissions

Second, the relationship between TI and combustion characteristics was examined. τ_{fi} , combustion period, and maximum ROHR were taken as the characteristics, and τ_{fi} was quantitatively redefined here on ASOE basis as the time when 5% of supplied fuel energy released in the MC, and the combustion period is as the duration from τ_{fi} to the timing when 95% of supplied energy released. As shown in (b) and (c), strengthening TI led to a proportional increase in τ_{fi} and the maximum ROHR and to rather exponential shortening of the combustion period. So, TI is thought to be effective to quantify the extension of ignition delay due to turbulent mixing and the subsequent combustion promotion.

Finally, the unburned fuel component (CH_4) and NO_x in the MC residual gas were taken as the emission characteristics of the combustion in the MC. The unburned fuel emission was negatively correlated with TI and NO_x emission was positively and exponentially correlated with TI. Again, TI can indicate a degree of the combustion promotion by the ejecting strength of torch flames from a PC.

Overall, TI could be used to organize the combustion results in the CVC, but, before applying it to real engines, it is necessary to investigate the effects of engine speed and the trade-off between the combustion promotion and increased cooling loss caused by the torch flame impinging on the inner wall of the MC.

5. Conclusions

Combustion experiments were conducted by supplying methane-air premixture separately to the prechamber and main chamber of a constant-volume chamber simulating a prechamber-type medium-speed gas engine and changing the orifice specifications to investigate their effects on the combustion process in the main chamber and the effectiveness of the torch flame strength to organize the results. The following conclusions were derived.

(1) In the early stage of combustion after the premixture has ignited around the torch flame, the combustion of the premixture in the main chamber entrained into the torch flame is predominant. Flame propagation to the unburned premixture then becomes predominant from the middle to late stage.

(2) The ignition of the entrained premixture accompanies the secondary ignition delay in the main chamber from the torch flame to the premixture and the ignition delay distance that the torch flame penetrates alone from the orifice exit during that ignition delay. The combustion progresses mainly in a direction that increases the spreading angle of the torch flame instead of a direction that increases the torch flame penetration in the early stage of the combustion.

(3) A short ignition delay in the main chamber tends to transition the torch flame to a snake-head profile and cause

the rapid decay of penetrating momentum, resulting in slow combustion in the end gas zone.

(4) When the total orifice opening area is kept constant, the number of orifices has little effect on the ignition delay in the main chamber nor the heat release process in the main chamber because of the trade-off between the combustion promotion by the increase in ejection momentum per torch flame and the hindrance by the decrease in flame surface area and the increase in the gap between torch flames. The appropriate number of orifices is limited to a narrow range.

(5) When the number of orifices and the prechamber volume are kept appropriate, with high ejection velocity of the torch flames by a small orifice diameter, the above-mentioned ignition delay and ignition delay length are elongated, but the following combustion promotion around the torch flame and in the end gas zone in the main chamber more than compensates for these drawbacks. Conversely, with very slow ejection velocity by a large orifice, as mentioned in (3), it has proven difficult to completely burn up the premixture in the end gas zone of the main combustion chamber.

(6) When the ignition delay in the main combustion chamber extends because of the high ejection velocity of the torch flame, the ignition position changes and the variation in ignition delay between torch flames increases. The latter may lead to the formation of a secondary in-chamber flow, which may increase the variation in the combustion process for each torch flame, which may be the cause of the large cyclic variation in actual gas engines.

(7) CFD incorporating a RANS-type turbulence model and detailed chemical reactions, which successfully reproduced the ejection behaviour of the torch flame when nitrogen was filled in the main chamber, is insufficient to reproduce the combustion process in the main chamber, except in cases where the torch flame ejection velocity is very low. The simulation for prechamber-type gas engines needs appropriate sub-models that reflect the quenching and ignition fluctuation due to turbulent mixing as well as the combustion-promotion by the torch flame jet.

(8) The existing formula proposed for estimating flame jet intensity in a high-speed small engine was applied to the measurement results of the study and found to have enough validity through checking the correlation with the penetration length of the torch flame, the heat release process in the main chamber, and the emission characteristics.

As a future task, additional measurements are necessary to verify the generality of these conclusions, as well as to investigate the effects of turbulent flow fields existing in an actual engine. For numerical predictions, it is necessary to reproduce the above-mentioned effects by turbulent mixing.

Nomenclature

A total cross-sectional opening area of flow paths
AFR air-to-fuel ratio
AMR adaptive mesh refinement
APC active pre-combustion chamber
ASOE after the start of a torch flame ejection

CFD computational fluid dynamics
CPU central processing unit
CVC constant-volume chamber
D diameter of a chamber/window or a flow path
GRI The Gas Research Institute

| | | | |
|-----------------|---|---------|---|
| H | height of a chamber/window or a flow path | RNG | renormalization group |
| HG | greenhouse gas | ROHR | rate of heat release |
| I _b | jet intensity proposed by Nada et al. [19] | SAGE | structural adaptive grid embedding |
| IMO | International Maritime Organization | TI | torch flame intensity |
| L | length of a flow path, penetration of a gas jet or distance between ignition position of MC pre-mixture on a torch flame and orifice exit of PC | θ | spreading full angle of a gas jet |
| Ĺ | flow speed or penetration speed of a gas jet | λ | global air excess ratio in a combustion chamber |
| LBGE | lean-burn premixed combustion gas engine | t | elapsed time on ASOE basis (see the last item) |
| N | number of flow paths | τ | delay time |
| MC | main combustion chamber, also used as a suffix | Subfix: | |
| MEPC | Marine Environment Protection Committee | f | torch flame |
| NG | natural gas | fi | ignition of MC pre-mixture by torch flame |
| NO _x | nitrogen oxides | max | maximum of ROHR |
| PC | pre-combustion chamber, also used as a suffix | o | PC orifice |
| RANS | Reynolds-Averaged Navier-Stokes equations | t | PC throat |
| | | W | optical window |

Bibliography

- [1] Aakko-Saksa T, Lehtoranta K, Kuittinen N, Järvinen A, Jalkanen J, Johnson K et al. Reduction in greenhouse gas and other emissions from ship engines: current trends and future options. *Prog Eng Combust.* 2023;94:101055. <https://doi.org/10.1016/j.pecs.2022.101055>
- [2] Al-Enazi A, Okonkwo EC, Bicer Y, Al-Ansari T. A review of cleaner alternative fuels for maritime transportation. *Energy Reports.* 2021;7:1962-1985. <https://doi.org/10.1016/j.egy.2021.03.036>
- [3] Aoyagi T, Wakasugi T, Tsuru D, Tashima H. Analysis of effects of pre-chamber orifices on torch flame behaviours in lean-burn gas engines. *Combustion Engines.* 2024;199(4):3-14. <https://doi.org/10.19206/CE-188112>
- [4] Babajimopoulos A, Assanis DN, Flowers DL, Aceves SM, Hessel RP. A fully coupled computational fluid dynamics and multi-zone model with detailed chemical kinetics for the simulation of premixed charge compression ignition engine. *Int J Engine Res.* 2005;6:497-512. <https://doi.org/10.1243/146808705X30503>
- [5] Brynolf S, Hansson J, Anderson JE, Skov IR, Wallington TJ, Grahn M et al. Review of electrofuel feasibility – prospects for road, ocean, and air transport. *Prog Energ.* 2022;4:4. <https://doi.org/10.1088/2516-1083/ac8097>
- [6] Bueschke W, Skowron M, Szwajca F, Wisłocki K. Flame propagation velocity in 2-stage gas combustion system applied in SI engine. *IOP Conf Ser: Mater Sci Eng.* 2018; 421:042009. <https://doi.org/10.1088/1757-899X/421/4/042009>
- [7] Bueschke W, Skowron M, Wisłocki K, Szwajca F. Comparative study on combustion characteristics of lean premixed CH₄/air mixtures in RCM using spark ignition and turbulent jet ignition in terms of orifices angular position change. *Combustion Engines.* 2019;176(1):36-41. <https://doi.org/10.19206/CE-2019-105>
- [8] Cho HM, He BQ. Spark ignition natural gas engines – a review. *Eng Convers Manage.* 2007;48(2):608-618. <https://doi.org/10.1016/j.enconman.2006.05.023>
- [9] Duan X, Deng B, Liu Y, Zou S, Liu J, Feng R. An experimental study the impact of the hydrogen enrichment on cycle-to-cycle variations of the large bore and lean burn natural gas spark-ignition engine. *Fuel.* 2020;282:118868. <https://doi.org/10.1016/j.fuel.2020.118868>
- [10] Einewall P, Johansson B. Cylinder to cylinder and cycle to cycle variations in a six cylinder lean burn natural gas engine. *SAE Technical Paper 2000-01-1941.* 2000. <https://doi.org/10.4271/2000-01-1941>
- [11] Guo H, Zhou S, Shreka M, Feng Y. Effect of pre-combustion chamber nozzle parameters on the performance of a marine 2-stroke dual fuel engine. *Processes.* 2019;7(12):876. <https://doi.org/10.3390/pr7120876>
- [12] IMO HP MEPC80. <https://www.imo.org/en/MediaCentre/PressBriefings/pages/Revised-GHG-reduction-strategy-for-global-shipping-adopted-.aspx>
- [13] Ishibashi R, Tsuru D. An optical investigation of combustion process of a direct high-pressure injection of natural gas. *J Mar Sci Technol.* 2017;22:447-458. <https://doi.org/10.1007/s00773-016-0422-x>
- [14] Kazakov A, Frenklach M. GRI-Mech. University of California at Berkeley. <http://combustion.berkeley.edu/drm/>
- [15] Korakianitis T, Namasivayam AM, Crookes RJ. Natural-gas fueled spark-ignition (SI) and compression-ignition (CI) engine performance and emissions. *Prog Eng Combust.* 2011;37(1):89-112. <https://doi.org/10.1016/j.pecs.2010.04.002>
- [16] Kulzer AC. Sustainability & powertrain systems: from electrification to hydrogen and efuels (updated). *Proc JSAE PEL Int Meeting, Technical Challenges for a Carbon Neutral Society by 2050. Keynote 4, Kyoto 2023.*
- [17] Liu J, Ulishney CJ, Dumitrescu CE. Experimental investigation of a heavy-duty natural gas engine performance operated at stoichiometric and lean operations. *Eng Convers Manage.* 2021;243(x):114401. <https://doi.org/10.1016/j.enconman.2021.114401>
- [18] Liu L, Wu Y, Wang Y. Numerical investigation on knock characteristics and mechanism of large-bore natural gas dual-fuel marine engine. *Fuel.* 2022;310:122298. <https://doi.org/10.1016/j.fuel.2021.122298>
- [19] Nada Y, Kidoguchi Y, Yamashita Y, Furukawa R, Kaya R, Nakamo H et al. Effects of sub-chamber configuration on heat release rate in a constant volume chamber simulating lean-burn natural gas engines. *SAE Int J Adv & Curr Prac in Mobility.* 2020;2(2):1032-1040. <https://doi.org/10.4271/2019-32-0551>
- [20] Pielecha I. Analysis of mass transfer in marine engine with prechamber combustion spark ignition system. *Bull Pol Ac: Tech.* 2021;69(2):e136744. <https://doi.org/10.24425/bpasts.2021.136744>
- [21] Pielecha I, Bueschke W, Skowron M, Fiedkiewicz Ł, Szwajca F, Cieślak W et al. Prechamber optimal selection for a two stage turbulent jet ignition type combustion system in

- CNG-fuelled engine. Combustion Engines. 2019;176(1):16-26. <https://doi.org/10.19206/CE-2019-103>
- [22] Senecal PK, Pomraning E, Richards KJ, Briggs TE, Choi CY, McDavid RM et al. Multi-dimensional modeling of direct-injection diesel spray liquid length and flame lift-off length using CFD and parallel detailed chemistry. Journal of Engines. 2003;112(3):1331-1351. <http://www.jstor.org/stable/44741357>
- [23] Shapiro E, Tiney N, Kyrtatos P, Kotzagianni M, Bolla M, Boulouchos K et al. Experimental and numerical analysis of pre-chamber combustion systems for lean burn gas engines. SAE Technical Paper 2019-01-0260. 2019. <https://doi.org/10.4271/2019-01-0260>
- [24] Shi J, Zhu Y, Feng Y, Yang J, Xia C. A prompt decarbonization pathway for shipping: green hydrogen, ammonia, and methanol production and utilization in marine engines. Atmosphere. 2023;14(3):584. <https://doi.org/10.3390/atmos14030584>
- [25] Tashima H, Kunimitsu M, Sugiura K, Tsuru D. Development of high-efficiency gas engine through observation and simulation of knocking phenomena. Proc CIMAC Congress 10 Bergen. 2013; No. 213.
- [26] Validi AA, Schock H, Jaber F. Turbulent jet ignition assisted combustion in a rapid compression machine. Combust Flame. 2017;186:65-82. <https://doi.org/10.1016/j.combustflame.2017.07.032>
- [27] Wakasugi T, Tsuru D, Tashima H. Influences of the pre-chamber orifices on the combustion behavior in a constant volume chamber simulating pre-chamber type medium-speed gas engines. Combustion Engines. 2022;191(4):66-76. <https://doi.org/10.19206/CE-148171>
- [28] Yasueda S, Takasaki K, Tashima H. The abnormal combustion affected by lubricating oil ignition in premixed gas engine. Proc ASME 2012 ICES. 2012:29-36. <https://doi.org/10.1115/ICES2012-81042>
- [29] Yuan M, Thellufsen JZ, Lund H, Liang Y. The electrification of transportation in energy transition. Energy. 2021; 236:121564. <https://doi.org/10.1016/j.energy.2021.121564>

Takahide Aoyagi, MEng. – Energy Conversion Group, Technology Platform Center, Technology & Intelligence Integration, IHI Corporation. Japan.
e-mail: t.jr.aoyagi@gmail.com



Daisuke Tsuru, DEng., Assoc. Prof. – Shipping Technology Department, National Institute of Technology (KOSEN), Oshima College, Japan.
e-mail: tsuru.daisuke@oshima.kosen-ac.jp



Takuya Wakasugi, MEng. – Interdisciplinary Graduate School of Engineering Sciences (IGSES), Kyushu University, Japan.
e-mail: wakasugi.takuya.875@s.kyushu-u.ac.jp



Hiroshi Tashima, DEng., Assoc. Prof. – Faculty of Arts and Sciences, Kyushu University, Japan.
e-mail: tajima.hiroshi.539@m.kyushu-u.ac.jp

